Journal of Metals, Materials and Minerals, 34(3), 2041, 2024

Effects of oleylamine concentration on the synthesis of formamidinium lead halide perovskite nanocrystals and physical-optical properties

Kunlasatree KUNSAENG[1,2], and Yingyot INFAHSAENG[1,2,*]

[1] *Division of Physics, Faculty of Science and Technology, Thammasat University, Pathum Thani, Thailand, 12120*
[2] *Thammasat University Research Unit in Quantum Technology, Thammasat University, Pathum Thani, Thailand, 12120*

***Corresponding author e-mail**: yingyot@tu.ac.th

Received date:
26 April 2024
Revised date:
24 June 2024
Accepted date:
13 July 2024

Keywords:
Perovskite nanocrystals;
LARP;
Organic ligands;
$FAPbBr_3$

Abstract

Perovskite nanocrystals (PNCs) has been extensively interested owing to their distinctive properties for applications in optoelectronics and energy harvesting. The properties of these nanocrystals, including optical and energy characteristics, can be tuned by adjusting the particle size using different synthesis techniques. Among these, the ligand-assisted reprecipitation (LARP) method has become popular for its simplicity and scalability. Nevertheless, it is vital to understand that the growth of PNCs is extremely sensitive to the conditions of synthesis, highlighting the importance of recognizing the factors that limit the formation and properties of PNCs. In this study, PNCs based on formamidinium lead bromide ($FAPbBr_3$) were synthesized via the LARP method under room temperature and ambient atmospheric conditions. The structures and optical properties, including photoluminescence lifetime, of PNCs with varying amounts of organic ligands were investigated. Transmission electron microscopy showed that high concentrations of organic ligands lead to the formation of perovskite clusters. We also noted a slight red shift in the photoluminescence peak as the size of the PNCs increased. A peak photoluminescence quantum yield (PLQY) of 74% was achieved. This study provides crucial insights into the effects of ligand ratios and serves as a valuable resource for refining the synthesis parameters of PNCs.

1. Introduction

Perovskite nanocrystals (PNCs) materials have extensively attracted the researchers' attention owing to their distinctive properties for optoelectronics and energy harvesting applications such as novel solar cells, light emitting diode, and photodetectors. [1-5]. One fascinating application is a single photon source which is important part for quantum technology [6,7]. The simple perovskite structure is ABX_3, where A is organic or inorganic material such as Cs^+, CH_3NH_3 (MA, methylammonium), or $CH(NH_2)_2$ (FA, formamidinium), B is metal cation such as Pb^{2+}, Sn^{2+}, or Cu^{2+}, and X is halide ion such as Cl, Br, I, or their mixture. Such perovskite structures exhibit the various excellence characteristics including high absorption coefficient, size-dependent photoluminescence, narrow emission spectra, tunability of their energy gap, and high quantum yield [3,8]. Among of perovskite nanocrystal materials, hybrid halide perovskite is one of interested materials due to the properties of organic semiconductors as well as those of the inorganic. Particularly, formamidinium lead halide perovskite nanocrystals feature attractive properties, for example, high stability against heat, light, and moisture, wide tunable emission in the range of 470 nm to 540 nm, and ease of synthesis under room temperature and ambient condition [9-13]. The synthesis of perovskite nanocrystals at low temperatures, particularly at room temperature, and under atmospheric conditions is crucial for several reasons. Firstly, the room temperature synthesis helps in deducing defects of nanocrystal structure and enhancing the photoluminescence quantum yields (PLQY) of the nanocrystals [14,15]. Furthermore, the synthesis of nanocrystals at room temperature and under ambient conditions presents a greener and safer alternative, eliminating the need for high temperatures and harmful solvents. This approach paves the way for simplified, economical, and scalable production processes [16,17]. Thus, room temperature and atmospheric condition synthesis methods play an important role in enhancing the optoelectronic properties, stability, and sustainability of perovskite nanocrystals, making them suitable for a wide range of applications.

In general, the absorption edge and photoluminescence (PL) peak of perovskite material shifted to the blue when decreasing the size of the nanoparticle due to quantum confinement effect. For several years, there are much approach of nanocrystal synthesis method with precise control of nanocrystal size, shape, and composition. Consequently, the synthesis of nanocrystal that are both high-quality and uniformly sized is essential for enhancing optical and energy properties, as well as facilitating their application in optoelectronics. Up to date, perovskite nanocrystals have been well-defined synthesized using several methods such as the hot-injection method [18,19], the microreactor method [9,20], the wet ball milling [21], the ultrasonic-assistant method [22], or the ligand-assisted reprecipitation method (LARP) [3,9,23-25]. The latter approach is a convenient and cost-effective method when conducted in ambient conditions at room temperature. Generally, the perovskite precursor, organic ligand, and a polar solvent are combined

to form the precursor solution, which is subsequently introduced into a nonpolar solvent. However, it is essential to thoroughly control various critical parameters in LARP, including precursor concentration, solvent, humidity, centrifugal speed, ligand type, or ligand ratio [26-28]. It is well known that capping ligands have been utilized for several decades to fabricate 2D perovskite materials. In the synthesis of perovskite nanocrystals, two common types of ligands, namely carboxylic acids, and amines, are typically utilized. It was assumed that carboxylic acids are employed to prevent aggregation effects of nanocrystals, whereas amines are used to regulate both the crystallization process and the size of the nanocrystals [4,13,29,30].

For instance, a binary ligand consisting of oleylamine, and oleic acid was employed in the room temperature synthesis of $CsPbBr_3$. The nanocrystal size of ~10 nm to 13 nm was controlled by the ligand [19]. Apart from oleylamine, octylamine was employed as a ligand. The resulting perovskite quantum dots were subsequently purified through differential centrifugation in a nonpolar solvent to achieve size selection [31]. Schmidt reported the synthesis of highly crystalline $MAPbBr_3$ nanocrystals, which were 6 nm in sized as nanoparticles. This was achieved using a longer chain alkyl ammonium cation as a capping ligand [18]. A highly luminescent colloidal $MAPbX_3$ quantum dot (average diameter 3.3 nm) was fabricated using n-octylamine and oleic acid in analytical-grade N, N-dimethylformamide (DMF) [3]. Although perovskite nanocrystals such as $MAPbX_3$ or $CsPbX_3$ are mostly synthesized by the ligand-assisted reprecipitation method, the synthesis of formamidinium lead halide ($FAPbX_3$) is much more challenging by the same technique. Zhao *et al.* replaced long-chain oleic acid ligands with short aromatic molecules of 2-naphthalenesulfonic acid in the $FAPbBr_3$ synthesis process and demonstrated higher photoluminescence quantum yield and lifetime [32]. Compared to previous studies, Levchuk demonstrated a facile and rapid strategy to synthesize $FAPbX_3$ nanocrystals at room temperature in ambient air, with an average humidity of ~45%. Nanocrystals ranging from 14 nm to 22 nm in size and exhibiting a nearly cubic shape were obtained. This synthesis was facilitated by a binary ligand comprising oleylamine and oleic acid, with anhydrous DMF used as the polar solvent [33]. Typically, $FAPbX_3$ nanocrystals are synthesized using traditional PbX_3 precursors; however, PbX_2-dimethyl sulfoxide (PbX_2-DMSO) complexes can serve as alternative precursors. In case of the PbX_2−DMSO complex, the DMSO ligand, acting as a Lewis base, can be easily replaced by the alkylammonium halide, a stronger Lewis base, at room temperature. This occurs through a direct intramolecular exchange reaction, which aids in the passivation of defects such as undercoordinated Pb^{2+} ions [34,35]. Moreover, the use of DMSO in the synthesis of perovskite quantum dots has been shown to produce uniform-sized nanocrystals with excellent luminescent properties, further supporting its potential in optoelectronic devices [36]. In the earlier study, the adjustment of oleylamine quantity facilitated the tuning of photoluminescence, transitioning from the blue to the near-infrared region [9]. In previous research, the quantity of acid ligand surpassed that of the amine ligand, resulting in an acid-to-amine ratio is greater than one. As the amount of amine increased, the nanocrystal size deceased, and photoluminescence shift towards the blue region. Nevertheless, Almeida demonstrated an increase in the size of nanocubes with the increasing of oleylamine amount [37]. Although, most perovskite synthesis parameters have been carefully controlled, some elements such as impurities of precursor and solvent hinder the crystallization of nanocrystals. A challenge in perovskite synthesis is the sensitivity to humidity and water-containing solvents. Nevertheless, Liu successfully incorporated water in the $MAPbBr_3$ synthesis process, leading to a significant enhancement in photoluminescence quantum yield from 2.5% to 71.54% [38].

In this work, we synthesize $FAPbBr_3$ nanocrystals in ambient air at room temperature using ligand assisted reprecipitation method. The impact of oleylamine concentration on the crystals size and photoluminescence was investigated. The 523 nm emission was achieved at lowest acid-to-amine ratio and slightly red shifted due to the increasing of nanocrystals size. We suggest that the limitation of ligand ratio and impurity of non-polar solvent are crucial to the perovskite synthesis strategy.

2. Experimental

2.1 Materials

$PbBr_2$ (98%, Sigma - Aldrich), Formamidine acetate (≥98%, TCI), Hydrobromic acid (HBr, 48%, Sigma - Aldrich), Dimethyl sulfoxide (≥99.5%, Daejung), N,N-dimethylformamide (DMF, analytical grade 99.8%, LOBA CHEMIE PVT), Toluene (≥95%, Fisher Scientific), Chlorobenzene (AR, RCI Labscan), Chloroform (AR, RCI Labscan), Oleylamine (OLA, technical grade 70%, Sigma - Aldrich), Oleic acid (OLAc, ≥99%, Sigma - Aldrich)

2.2 Synthesis of lead bromide-dimethyl sulfoxide ($PbBr_2$-DMSO)

The synthesis of $PbBr_2$-DMSO is an important step because this precursor solution can readily react with other components without need the high-temperature reaction or multiple procedures. To synthesize $PbBr_2$-DMSO, 1 g of $PbBr_2$ was dissolved in 7 mL of DMSO at 70°C, then precipitated by slowly adding 20 mL of toluene with vigorous stirring. The resulting white precipitate was filtered and dried for 3 h at room temperature. The final $PbBr_2$-DMSO powder was obtained through annealing at 60°C for 24 h under vacuum.

2.3 Synthesis of formamidinium bromide (FABr)

Formamidinium bromide was synthesized following the previous report [39]. To synthesize FABr, 10.41 g of formamidinium acetate powder was dissolved in 20 mL of HBr (48% w/w) solution, then stirred at 50°C for 10 min. After drying at 100°C for 2 h, a yellow-white power was washed with diethyl ether and recrystallized in ethanol. Before use, the powder was dried overnight in a vacuum oven.

2.4 Synthesis of formamidinium lead bromide ($FAPbBr_3$) nanocrystals

All syntheses were carried in ambient air at room temperature with an average humidity of ~45%. To synthesize $FAPbBr_3$ nanocrystals, the precursor solution was initially prepared by combining

$PbBr_2$-DMSO (0.1 M), FABr (0.1 M), and OLA (0 µL, 10 µL, 20 µL, and 30 µL) in 7 mL of DMF. The precursor solution was then slowly added dropwise into a mixture of toluene (175 mL) and OLAc (787 µL) under vigorous stirring as shown in Figure 1. Upon mixing with toluene, the solution immediately turned pale green. Finally, any large particles were removed from the $FAPbBr_3$ nanocrystal solution through centrifugation at 7000 rpm.

2.5 Characterization methods

The Fourier-transform infrared spectroscopy (FTIR) was carried out using the Bruker Invenio FTIR Spectrometer, covering a wavelength range from 80 cm^{-1} to 5000 cm^{-1}. X-ray diffractometer (XRD) measurement was performed using a Bruker D2 PHASER with CuK_α radiation (1.5046 Å). A small amount of perovskite precipitates after centrifugation was drop casted onto a quartz glass substrate and dried at room temperature for measurement. Transmission electron microscopy (TEM) measurements were conducted by JEOL 2100 Plus TEM machine operating at 200 kV. TEM samples were prepared by drop-casting onto a standard copper grid and allowing 24 h for drying. The size distribution of nanocrystals was determined from TEM images using ImageJ software. UV-Vis absorption spectra and photoluminescence (PL) of nanocrystal colloidal were performed using the Duetta spectrometer (HORIBA) with a 75 W Xenon arc lamp as the light source. For emission spectra, the excitation was carried out at 370 nm. Time-resolved photoluminescence (PL) measurements were performed using a spectrofluorometer equipped with time-correlated single photon counting (TCSPC) for lifetime measurements (FluoroMax Plus, HORIBA). Excitation was achieved using a nano-second LED emitting at a wavelength of 370 nm.

3. Results and discussion

The $FAPbBr_3$ nanocrystal was synthesized by ligand-assisted reprecipitation method. $PbBr_3$-DMSO and FABr were used as precursors and analytical grade DMF is utilized as the polar solvent. The synthesized $FAPbBr_3$ colloidal with various oleylamine amount were characterized by FTIR as shown in Figure 2. In the case of pure toluene, characterized as a non-polar solvent, the stretching and bending vibrations of C-H appear in the spectral range of 2800 cm^{-1} to 3200 cm^{-1} and 660 cm^{-1} to 760 cm^{-1}, respectively. Additionally, the C-C stretching in the aromatic ring of toluene exhibits multiple peaks within the range of 1400 cm^{-1} to 1600 cm^{-1}. The synthesis of $FAPbBr_3$ nanocrystals in toluene may results in the formation of a coordinate bond between formamidinium and toluene. This bonding may cause the peak shift of C-C stretching to the higher wavenumber. In the presence of $FAPbBr_3$, a peak appears around 1680 cm^{-1}. This peak is most likely attributed to the C=O stretching vibration, suggesting the oxidation of oleylamine (OLA) during the synthesis process [40]. While a less likely possibility, this peak could also be due to a shift in the C=N stretching vibration of the FA^+ cation resulting from its interaction with OLA [41.42]. At the same time, the presence of perovskite weakens the stretching and bending of C-H bonds. The observed decrease in intensity of the C-H bending vibrations (660 cm^{-1} to 760 cm^{-1}) of toluene with increasing OLA concentration suggests a competitive adsorption process, where OLA

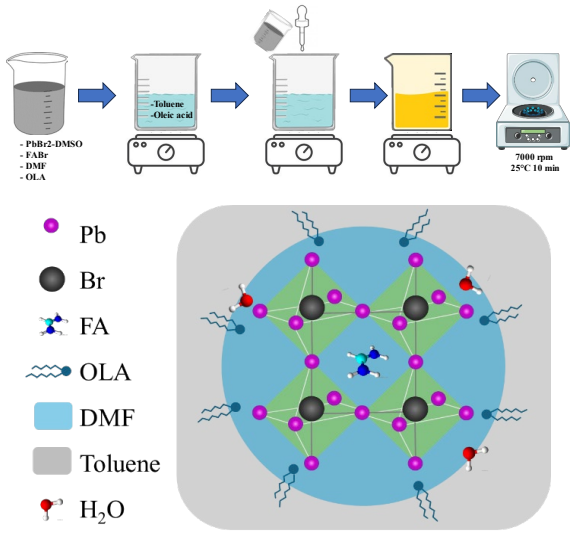

Figure 1. Schematic illustration of the $FAPbBr_3$ synthesis process and crystal structure.

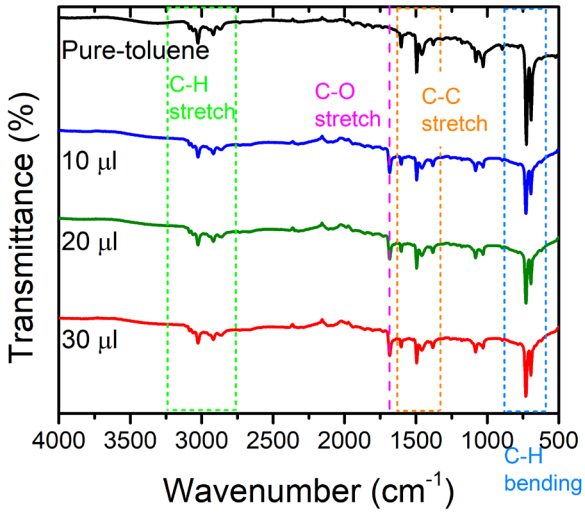

Figure 2. FTIR spectra of $FAPbBr_3$ synthesized with varying amounts of oleylamine (OLA): 10 µL, 20 µL, and 30 µL.

molecules displace toluene from the surface of the $FAPbBr_3$ nanocrystals. This displacement alters the solvent environment surrounding the nanocrystals, leading to a reduced number of toluene molecules in close proximity and a consequent decrease in the intensity of their characteristic C-H bending modes. To study the crystal structure of $FAPbBr_3$ nanocrystals, XRD analysis was carried out as shown in Figure 3. The results for $FAPbBr_3$ nanocrystals synthesized with 20 µL of OLA show the characteristic peaks at 14.9°, 21.1°,29.9°, 33.6°, 36.8°, 42.8° and 45.5°. These peaks can be attributed to the (100), (110), (200), (210), (211), (220) and (300) planes of the cubic $FAPbBr_3$ crystal structure, respectively, which is consistent with previous work [9,25]. The average unit cell parameter of the cubic phase was 5.958 Å, similar to that of bulk $FAPbBr_3$ perovskite [10,12]. This result confirmed the single phase of $FAPbBr_3$ with the space group of Pm-3m. The broad peak centered at ~25° was observed, which is the large size of the particulates. This suggest that the as-prepared precipitates are polycrystalline. The XRD patterns for nanocrystals synthesized with 10 µL and 30 µL of OLA are identical,

indicating that the synthesized nanocrystals have the same phase and structure. Thus, the $FAPbBr_3$ nanocrystal structure was not affected by the amount of OLA. However, a complex phase is observed in the $FAPbBr_3$ synthesized without OLA. The peaks labeled with a star indicate the $FAPbBr_3$ structure, while the peaks labeled with a diamond symbol are likely attributable to $PbBr_2$-DMSO complex remaining from an incomplete synthesis process [43]. The crystalline size of perovskite precipitates was calculated using the Debye-Scherrer equation, showing a mean size of 42.6 nm ± 9 nm, 41 nm ± 5 nm, and 42.7 nm ± 12 nm for the precipitates synthesized with 10 µL, 20 µL, and 30 µL of OLA, respectively. Note that these crystalline sizes were obtained from the XRD results of the perovskite precipitates, not the nanocrystals.

From high magnification transmission electron microscopy (TEM) image (Figure 4), the polydispersity of $FAPbBr_3$ nanocrystals were observed, which may arise from the aggregation. This suggests there may be room for further optimization of the organic ligand's ability to confine the nanocrystal size. As shown in Figure 4(a-c), $FAPbBr_3$ nanocrystals were mostly spherical shape. In addition, the lattice spacing of 0.259 nm showed in the Figure 4(d) of TEM image corresponds to (210) plane of $FAPbBr_3$ nanocrystals (d = 0.267 nm) and previous works [25,44]. However, TEM image of Figure 4(e) reveals cubic $FAPbBr_3$ nanocrystals with sizes ranging from 10 nm to 20 nm. As the OLA amount increases, an average diameter of nanocrystals slightly increases. The particle size distribution of nanocrystals was determined using a histogram generated with ImageJ software [45]. Size analysis of perovskite nanocrystals is shown in Figure 5, with average sizes of 2.7 nm ± 0.1 nm, 3.1 nm ± 0.1 nm, and 3.5 nm ± 0.1 nm for the 10 µL, 20 µL, and 30 µL of OLA, respectively. Compared to the Bohr exciton radius of $FAPbBr_3$ (~8 nm) in previous work [25], all synthesized $FAPbBr_3$ nanocrystals have smaller diameters. Thus, these nanocrystals fall within the strong quantum confinement regime, where the size of the nanocrystals is significantly smaller than the Bohr exciton diameter. Typically, adding more OLA results in the formation of smaller nanocrystals because OLA serves as a capping agent, attaching to the nanocrystal surfaces and inhibiting further growth. However, the presence of water and moisture can disrupt this process. OLA may react with water to produce oleylamine hydrochloride, thereby decreasing the amount of free OLA available for capping. This reduction can lead to larger nanocrystals as the decrease in available OLA compromises growth regulation. In cases where perovskite nanocrystals were synthesized without oleylamine (OLA), a TEM image of the colloidal solution could not be obtained due to the absence of $FAPbBr_3$ nanocrystals. However, the precipitate showed the presence of a substance (Figure 4(f)). These substances may be $FAPbBr_3$ and $PbBr_2$-DMSO, which is consistent with the XRD results. Note that the perovskite synthesis in this work was conducted at room temperature and under ambient atmospheric condition with a humidity level of ~50%. The chemical used was not purified and may contain a high percentage of water. However, we have observed that higher OLA concentrations can form the $FAPbBr_3$ nanocrystals with a larger average diameter while still exhibiting their photoluminescent properties.

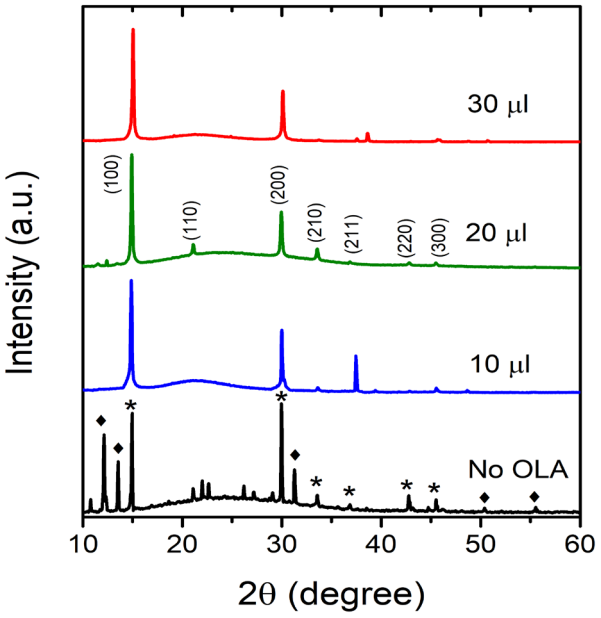

Figure 3. XRD pattern of the precipitate collected from the centrifuged $FAPbBr_3$ nanocrystal solution.

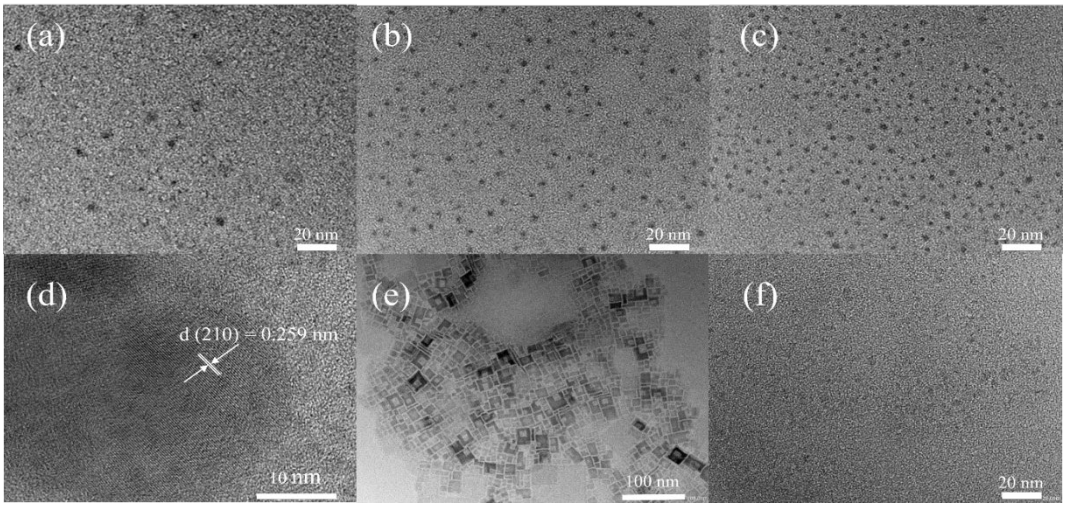

Figure 4. TEM images of $FAPbBr_3$ nanocrystals synthesized with varying amounts of oleylamine (OLA): (a) 10 µL, (b) 20 µL, and (c) 30 µL. (d) high-resolution TEM image of a single $FAPbBr_3$ nanocrystal showing interplanar spacing. (e) aggregation of cubic $FAPbBr_3$ nanocrystals. (f) high-resolution TEM image of $FAPbBr_3$ synthesized without OLA.

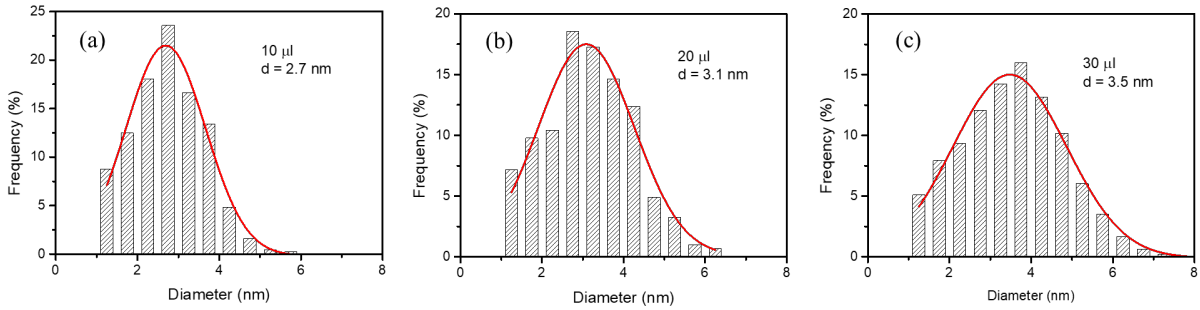

Figure 5. Size distributions of $FAPbBr_3$ nanocrystals synthesized with different amounts of oleylamine (OLA): (a) 10 µL, (b) 20 µL, and (c) 30 µL.

As shown in Figure 6(a), $FAPbBr_3$ nanocrystals exhibit a color change under different lighting conditions. At room temperature, they appear yellowish in ambient light, but transform to a pale green color when exposed to a UV lamp. The ultraviolet-visible (UV-vis) absorption and photoluminescence (PL) spectra of the $FAPbBr_3$ nanocrystals with varying amounts of OLA are shown in Figure 6(b). The absorption spectra exhibit a first transition at ~550 nm. The absorption band becomes broader and less defined as the amount of OLA increases. This is likely due to the low concentration of perovskite nanocrystals in the solution, which increases the signal-to-noise ratio. For the 30 µL OLA condition, sub-bandgap absorption is observed at wavelengths greater than approximately 525 nm. This phenomenon can be attributed to aggregation-induced light scattering. Furthermore, the weak absorption peaks observed at 430 nm and 475 nm in both the 20 µL and 30 µL OLA conditions may be attributed to the presence of surface defects and impurities within the $FAPbBr_3$ samples such as vacancies or dangling bonds during synthesis. The energy band gaps (E_g) were calculated using Tauc's method and found to be 2.33 eV, 2.22 eV, and 2.01 eV for the OLA conditions of 10 µL, 20 µL, and 30 µL, respectively. Additionally, the $FAPbBr_3$ solution formed without OLA exhibits an energy band gap of 2.24 eV, which is close to the bulk energy gap [39]. The measured PL spectra are red-shifted from 523 nm to 531 nm with the increasing average size diameter of $FAPbBr_3$ nanocrystals as shown in Figure 6(b) and Table 1. The observed PL peaks are comparable to those of $FAPbBr_3$ nanocrystals reported in other studies [9,12,13]. A narrow full width at half maxima (FWHM) of approximately 40 nm is observed when using 10 µL and 20 µL of OLA amount. Interestingly, at 30 µL OLA, a new PL peak centered at ~417 nm appears in the PL spectra of $FAPbBr_3$ perovskite nanocrystals. This indicates the possible formation of small perovskite nanocrystals, with the excess ligand ratio potentially inhibiting further crystal growth. However, the particle size distribution of the nanocrystals at 30 µL OLA is relatively broad, suggesting that large particles may be significantly contributing to the PL spectra. In this case, the addition of OLA caused a red-shift in the PL, coinciding with the increase in the size of the $FAPbBr_3$ nanoparticles. For the perovskite solution formed without OLA, the PL peak is located at 540 nm and exhibits a narrow width of 23 nm. Nonetheless, the PL intensity of the $FAPbBr_3$ nanocrystals decreased rapidly, dropping by almost 50% within the first 48 h. However, a relative photoluminescence quantum yield (PLQY) of 74% was achieved for the nanocrystals synthesized with 20 µL OLA. The PLQY significantly decreased when 30 µL of OLA was used and was almost completely quenched for the $FAPbBr_3$ solution without OLA.

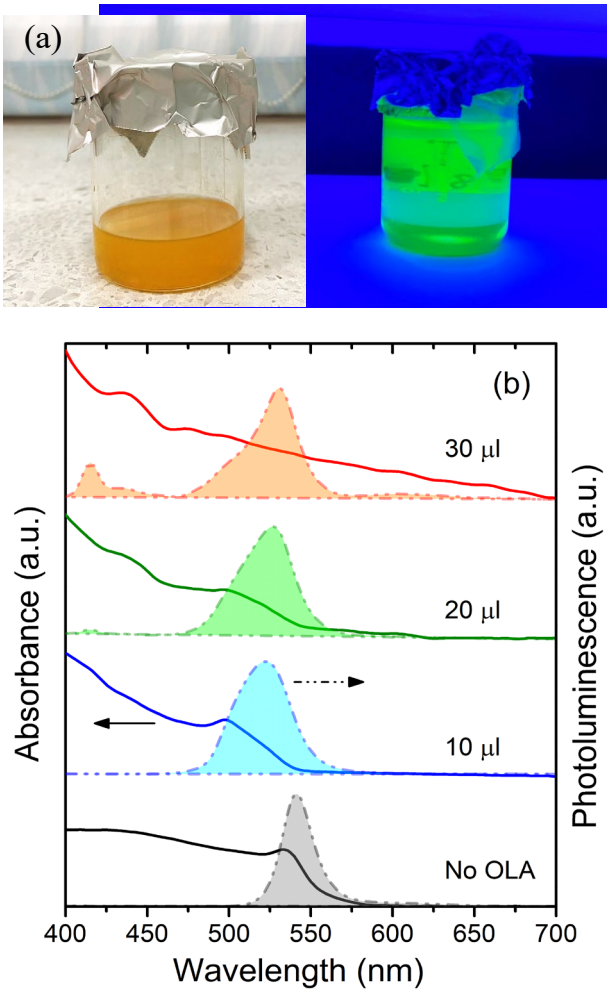

Figure 6. (a) Photographs of $FAPbBr_3$ nanocrystal solutions under ambient light and UV illumination. (b) Absorption (solid lines) and photoluminescence (PL) (dashed lines with shaded areas) spectra of $FAPbBr_3$ nanocrystal solutions synthesized without OLA and with 10 µL, 20 µL, and 30 µL of OLA.

Figure 7 shows the time-resolved PL traces of the $FAPbBr_3$ solution with added oleylamine ranging from 0 to 30 µL. A multi-exponential fit can be obtained for all traces. However, while single or bi-exponential decay functions have been used to fit the time-resolved PL traces of $FAPbBr_3$ nanoparticles and films [25,33,46], a tri-exponential function may also be employed. In bi-exponential fitting, the short lifetime is typically due to recombination facilitated by surface impurities and traps, whereas the longer lifetime arises from intrinsic band edge emission.

In this work, the PL decay curves are well represented by a tri-exponential function, with the lifetime values detailed in the inset of Figure 7, where A and τ are the amplitude components and lifetimes, respectively. The average lifetime (τ_{ave}) then is defined as $\tau_{ave} = \sum_{i=1}^{n} A_i\tau_i^2 / \sum_{i=1}^{n} A_i\tau_i$. As the amount of OLA increases, there is a noticeable extension in the lifetime, suggesting lower electron trap states. Specifically, the average lifetime of the $FAPbBr_3$ nanocrystal with 20 µL of OLA is 38.34 ns, which is longer compared to 25.98 ns when only 10 µL of OLA is used. Interestingly, the photoluminescence (PL) decay at 30 µL of OLA reveals a rapid component of approximately 1 ns, potentially indicative of a quenching process due to surface defects. However, an average lifetime of 39.77 ns was obtained, which correlates with the lower exciton binding energy typically found in large particle sizes [12]. In contrast, the average lifetime of the $FAPbBr_3$ solution formed without OLA is 3.34 ns. This lifetime is primarily dominated by a quenching decay of 1 ns, likely due to quenchers such as $PbBr_2$-DMSO. For the precipitates with 10 µL of OLA, the average PL lifetime is significantly longer than 1 ms, which is attributed to a lengthy charge diffusion length found in larger particles. The PL decay results demonstrate how the amount of OLA influences the synthesis of perovskite nanocrystals. From the TEM results, this strong quantum confinement typically leads to increased energy levels and altered optical properties, such as shorter photoluminescence (PL) lifetimes due to enhanced electron-hole recombination rates and a blue shift in emission wavelengths. Compare to the $FAPbBr_3$ solution formed without OLA, the PL peak or nanocrystals should be the PL peak of nanocrystals. Due to a larger energy separation between level and a decreasing of particle size, a faster radiative recombination and shorter PL lifetimes can be observed from the smaller $FAPbBr_3$ nanocrystals as shown in Table 1.

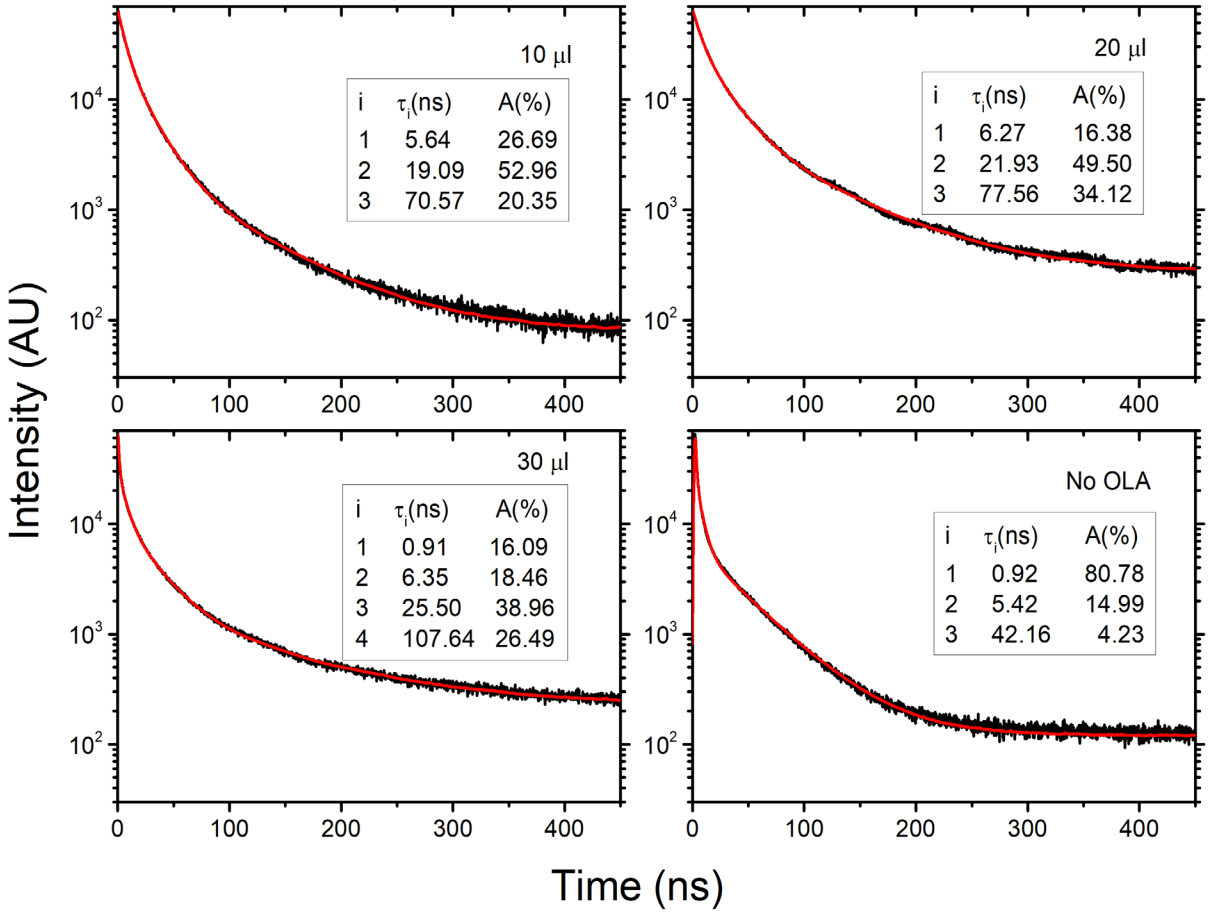

Figure 7. Time-resolved PL lifetimes of $FAPbBr_3$ solutions without OLA and with the addition of 10 µL, 20 µL, and 30 µL of oleylamine.

Table 1. Peak wavelength, full width at half maximum (FWHM) of PL spectra, photoluminescence quantum yield (PLQY), and energy band gap of $FAPbBr_3$ nanocrystals synthesized without OLA and with 10 µL, 20 µL, and 30 µL of OLA.

Oleylamine value (µL)	Particle size (nm)	PL Peak (nm)	FWHM (nm)	PLQY (%)	E_g (eV)	τ_{ave} (ns)
No OLA	-	540	23	2.88	2.24	3.34
10	2.7	523	40	72.29	2.33	25.98
20	3.1	527	40	74.06	2.22	38.34
30	3.5	531	39	51.23	2.01	39.77

4. Conclusions

In conclusion, we have successfully synthesized the $FAPbBr_3$ colloidal nanocrystals using varying amounts of oleylamine (OLA) at room temperature in an open-air environment. Consequently, perovskite nanocrystals synthesized with higher concentrations of OLA exhibit larger particles sizes, which can be attributed to water defects and moisture absorption in conditions of high humidity. The observed increase in particle size resulted in a red-shift of the photoluminescence (PL) peak, indicating a decrease in the bandgap energy. Additionally, the PL lifetime was extended, which can be attributed to reduced quantum confinement effects and a decrease in surface-to-volume ratio, leading to fewer non-radiative recombination pathways. A peak photoluminescence quantum yield (PLQY) of 74% was achieved with the addition of 20 µL of OLA during the synthesis process. Our work establishes criteria of organic ligand amounts for synthesizing perovskite nanocrystals and also demonstrates the impact of organic ligand and synthesis environment. To optimize the synthesis of $FAPbBr_3$ nanoparticles with high photoluminescence quantum yield, it is recommended to use less than 20 µL of the organic ligand oleylamine (OLA). This information is valuable for guiding researchers in designing these materials and exploring their potential applications in future optoelectronic devices.

Acknowledgements

This work was supported by Thammasat University Research Fund, Contact No.TUFT 46/2564, Thammasat University Research Unit in Quantum Technology and by the Thailand Science Research and Innovation Fundamental Fund fiscal year 2023.

Reference

[1] B. R. Sutherland, and E. H. Sargent, "Perovskite photonic sources," *Nature Photonics*, vol. 10, no. 5. 2016.

[2] K. Lin, J. Xing, L. N. Quan, F. P. Carcia de Arquer, X, Gong, J. Lu, L, Xie, W. Zhao, D. Zhang, C. Yan, W. Li, X. Liu, Y. Lu, J. Kirman, E. H. Sargent, Q. Xiong, and Z. Wei, "Perovskite light-emitting diodes with external quantum efficiency exceeding 20 per cent," *Nature*, vol. 562, no. 7726, pp. 245-248, 2018.

[3] F. Zhang, H. Zhong, C. Chen, X-g. Wu, X. Hu, H. Huang, J. Han, B. Zou, and Y. Dong, "Brightly luminescent and color-tunable colloidal $CH_3NH_3PbX_3$ (X = Br, I, Cl) quantum dots: Potential alternatives for display technology," *ACS Nano*, vol. 9, no. 4, pp. 4533-4542, 2015.

[4] H. Huang, L. Polavarapu, J. A. Sichert, A. S. Susha, A. S. Urban, and A. L. Rogach, "Colloidal lead halide perovskite nanocrystals: Synthesis, optical properties and applications," *NPG Asia Materials*, vol. 8, no. 11, 2016.

[5] M. V Kovalenko, L. Protesescu, and M. I. Bodnarchuk, "Properties and potential optoelectronic applications of lead halide perovskite nanocrystals," *Science,* vol. 10, no. 358, pp. 745-750, 2017.

[6] Y. S. Park, S. Guo, N. S. Makarov, and V. I. Klimov, "Room temperature single-photon emission from individual perovskite quantum dots," *ACS Nano*, vol. 9, no. 10, pp. 10386-10393, 2015.

[7] C. T. Trinh, D. N. Minh, K. J. Ahn, Y. Kang, and K. G. Lee, "Organic-inorganic $FAPbBr_3$ perovskite quantum dots as a quantum light source: single-photon emission and blinking behaviors," *ACS Photonics*, vol. 5, no. 12, pp. 4937-4943, 2018.

[8] Y. Li, T. Ding, X. Luo, Y. Tian, X. Lu, and K. Wu, "Synthesis and spectroscopy of monodispersed, quantum-confined $FAPbBr_3$ perovskite nanocrystals," *Chemistry of Materials*, vol. 32, no. 1, pp. 549-556, 2020.

[9] D. N. Minh, J. Kim, J. Hyon, J. H. Sim, H. H. Sowlih, C. Seo, J. Nam, S. Eom, S. Suk, S. Lee, E. Kim, and Y. Kang, "Room-temperature synthesis of widely tunable formamidinium lead halide perovskite nanocrystals," *Chemistry of Materials*, vol. 29, no. 13, pp. 5713-5719, 2017.

[10] E. Edri, S. Kirmayer, M. Kulbak, G. Hodes, and D. Cahen, "Chloride inclusion and hole transport material doping to improve methyl ammonium lead bromide perovskite-based high open-circuit voltage solar cells," *Journal of Physical Chemistry Letters,* vol. 5, no. 3, pp. 429-433, 2014

[11] A. Zhumekenov, M. Saodaminov, M. A. Haque, E. Alarousu, S. P. Sarmah, M. Banavoth, I. Dursun, Z-H. Miao, A. L. Abdelhady, T. Wu, O. F. Mohammed, and O. M. Bakr, "Formamidinium lead halide perovskite crystals with unprecedented long carrier dynamics and diffusion length," *ACS Energy Letters*, vol. 1, no. 1, pp. 32-37, 2016.

[12] L. Protesescu, S. Yakunin, M. I. Bodnarchuk, F. Bertolotti, N. Masciocchi, A. Guagliardi, and M. V. Kovalenko, "Monodisperse formamidinium lead bromide nanocrystals with bright and stable green photoluminescence," *Journal of the American Chemical Society*, vol. 138, no. 43, pp. 14202-14205, 2016.

[13] H. Bhatia, B. Ghosh, and E. Debroye, "Colloidal $FAPbBr_3$ perovskite nanocrystals for light emission: what's going on?," *Journal of Materials Chemistry C*, vol. 10, no. 37, pp. 13437-13461, 2022.

[14] S. R. Pathipati, M. N. Shah, S. Akhil, and N. Mishra, "In situ synthesis of high-quantum-efficiency and stable bromide-based blue-emitting perovskite nanoplatelets," *Nanoscale Advances*, vol. 4, no. 22, pp. 4766-4781, 2022.

[15] Y. Cai, P. Zhang, W. Bai, L. Lu, L. Wang, X. Chen, and R-J. Xie, "Synthesizing bright $CsPbBr_3$ perovskite nanocrystals with high purification yields and their composites with in situ-polymerized styrene for light-emitting diode applications," *ACS Sustainable Chemistry Engineering*, vol. 10, no. 22, pp. 7385-7393, 2022.

[16] S. Sansoni, F. M. Anoè, and M. Meneghetti, "Simple and sustainable synthesis of perovskite-based optoelectronic material: $CsPbBr_3$ nanocrystals via laser ablation in alcohol," *Nanoscale Advance*, vol. 4, no. 23, pp. 5009-5014, 2022.

[17] V. R. Yandri, P. Wulandari, and R. Hidayat, "Photoluminescence properties of $CsPbCl_3$ and $CsPbBr_3$ nanocrystals synthesized by LARP method with various ligands and anti-solvents," in *Journal of Physics: Conference Series*, Institute of Physics, 2022.

[18] L. C. Schmidt, A. Pertegas, S. Gonzalez-Carrero, O. Malinkiewicz, S. Agouram, G. M. Espallargas, H. Bolink, R. Galian, and J. Perez-Prieto, "Nontemplate synthesis of $CH_3NH_3PbBr_3$ perovskite nanoparticles," *Journal og the American Chemical Society*, vol. 136, no. 3, pp. 850-853, 2014.

[19] X. Li, Y. Wu, S. Zhang, B. Cai, Y. Gu, J. Song, and H. Zeng, "$CsPbX_3$ quantum dots for lighting and displays: roomerature synthesis, photoluminescence superiorities, underlying origins and white light-emitting diodes," *Advanced Functional Materials*, vol. 26, no. 15, pp. 2435-2445, 2016.

[20] K. Abdel-Latif, F. Bateni, S. Crouse, and M. Abolhasani, "Flow synthesis of metal halide perovskite quantum dots: from rapid parameter space mapping to AI-guided modular manufacturing," *Matter*, vol. 3, no. 4. *Cell Press*, pp. 1053-1086, 2020.

[21] L. Protesescu, S. Yakunin, O. Nazarenko, D. N. Dirin, and M. V. Kovalenko, "Low-cost synthesis of highly luminescent colloidal lead halide perovskite nanocrystals by wet ball milling," *ACS Appiedl Nano Materials*, vol. 1, no. 3, pp. 1300-1308, 2018.

[22] L. C. Chen, Z. L. Tseng, S. Y. Chen, and S. Yang, "An ultrasonic synthesis method for high-luminance perovskite quantum dots," *Ceramics International,* vol. 43, no. 17, pp. 16032-16035, 2017.

[23] L. Protesescu, S. Yakunin, M. I. Bodnarchuk, F. Krieg, R. Caputo, C. H. Hendon, R. X. Yang, A. Walsh, and M V. Kovalenko, "Nanocrystals of cesium lead halide perovskites ($CsPbX_3$, X = Cl, Br, and I): novel optoelectronic materials showing bright emission with wide color gamut," *Nano Letters*, vol. 15, no. 6, pp. 3692-3696, 2015.

[24] F. Krieg, S. T. Ochsenbein, S. Yakunin, S. t. Brinck, P. Aellen, A. Suess, B. Clerc, D. Guggisberg, O. Nazarenko, Y. Shynkarenko, S. Kumar, C-J. Shih, I. Infante, and M. V. Kovalenko, "Colloidal $CsPbX_3$ (X = Cl, Br, I) nanocrystals 2.0: Zwitterionic capping ligands for improved durability and stability," *ACS Energy Letters*, vol. 3, no. 3, pp. 641-646, 2018.

[25] A. Perumal, S. Shendre, M. Li, Y. K. E. Tay, V. K. Shrma, S. Chen, Z. Wei, Q. Liu, Y. Gao, P. J. S. Buenconsejo, S. T. Tan, C. L. Gan, Q. Xiong, T. C. Sum, and H. V. Demir, "High brightness formamidinium lead bromide perovskite nanocrystal light emitting devices," *Scientific Reports*, vol. 6, p. 36733, 2016.

[26] A. Prochazkova, S. Demchyshyn, C. Yumusak, J. Masilko, O. Bruggenmann, M. Weiter, M. Kaltenbrunner, N. S. Sariciftci, J. Krajcovic, Y. Salinas, A. Kovalenko, and A. Kovalenko, "Proteinogenic amino acid assisted preparation of highly luminescent hybrid perovskite nanoparticles," *ACS Applied Nano Materials*, vol. 2, no. 7, pp. 4267-4274, 2019.

[27] H. Huang, J. Raith, S. Kershaw, S. Kalytchuk, O. Tomanec, L. Jing, A. Susha, R. Sboril, and A. Rogach, "Growth mechanism of strongly emitting $CH_3NH_3PbBr_3$ perovskite nanocrystals with a tunable bandgap," *Nature Communications*, vol. 8, no. 1, 2017.

[28] A. Jancik Prochazkova, M. Scharber, C. Yumusak, J. Jancik, J. Masilko, O. Bruggemann, M. Weiter, N. S. Sariciftci, J. Krajcovic, Y. Salinas, and A. Kovalenko, "Synthesis conditions influencing formation of $MAPbBr_3$ perovskite nanoparticles prepared by the ligand-assisted precipitation method," *Scientific Reports*, vol. 10, no. 1, 2020.

[29] F. Haydous, J. M. Gardner, and U. B. Cappel, "The impact of ligands on the synthesis and application of metal halide perovskite nanocrystals," *Journal of Materials Chemistry A*, vol. 9, no. 41, *Royal Society of Chemistry*, pp. 23419-23443, 2021.

[30] S. Mourdikoudis, M. Menelaou, N. Fiuza, G. Zheng, S. Wei, J. Perez-Juste, P. Lakshminarayana, Z. Sofer, "Oleic acid/ oleylamine ligand pair: a versatile combination in the synthesis of colloidal nanoparticles," *Nanoscale Horizons*, vol. 7, no. 9, *Royal Society of Chemistry*, pp. 941-1015, 2022.

[31] S. Zhou, "Rapid separation and purification of lead halide perovskite quantum dots through differential centrifugation in nonpolar solvent," *RSC Advances*, vol. 11, no. 45, pp. 28410-28419, 2021.

[32] H. Zhao, H. Chen, S. Bai. C. Kuang, X. Luo, P. Teng, C. Yin, P. Zeng, L. Hou, Y. Yang, L. Duan, F. Gao, and M. Liu, "High-brightness perovskite light-emitting diodes based on $FAPbBr_3$ nanocrystals with rationally designed aromatic ligands," *ACS Energy Letters*, vol. 6, no. 7, pp. 2395–2403, 2021.

[33] I. Levchuk, A. Osvet, X. Tang, M. Brandl, J. D. Perea, F. Hoegl, G. J. Matt, R. Hock, M. Batentschuk, and C. J. Brabec, "Brightly luminescent and color-tunable formamidinium lead halide perovskite $FAPbX_3$ (X = Cl, Br, I) colloidal nanocrystals," *Nano Letters*, vol. 17, no. 5, pp. 2765-2770, 2017.

[34] J. W. Lee, H. S. Kim, and N. G. Park, "Lewis acid-base adduct approach for high efficiency perovskite solar cells," *Accounts of Chemical Research*, vol. 49, no. 2, pp. 311-319, 2016.

[35] W. S. Yang, J. Noh, N. Jeon, Y. C. Kim, S. Ryu, J. Seo, and S. Seok, "High-performance photovoltaic perovskite layers fabricated through intramolecular exchange," *Science (1979)*, vol. 348, no. 6240, pp. 1234-1237, 2015.

[36] J. Y. Kim, W. Jang, J. Lim, and D. H. Wang, "One-pot synthesis of all-inorganic $CsPbClBr_2$ blue perovskite quantum dots via stoichiometric precursor," *Inorganic chemistry*, vol. 62, no. 29, pp. 11665-11673, 2023.

[37] G. Almeida, L. Goldoni, Q. Akkerman, Z. Dang, A. H. Khan, S. Marras, I. Moreels, and L. Manna, "Role of acid-base equilibria in the size, shape, and phase control of cesium lead bromide nanocrystals," *ACS Nano*, vol. 12, no. 2, pp. 1704-1711, 2018.

[38] K. K. Liu, Q. Liu, Y. D. Wen, Y, Liang, L. Sui, J.-Y. Sui, J.-Y. Wei, G.-W. Xue, W.-B. Zhao, X.-Y. Wu, L. Dong, and C-X. Shan, "Water-induced $MAPbBr_3$@PbBr(OH) with enhanced luminescence and stability," *Light: Science and Applications*, vol. 9, no. 1, 2020.

[39] G. E. Eperon, S. D. Stranks, C. Menelaou, M. B. Johnston, L. M. Herz, and H. J. Snaith, "Formamidinium lead trihalide: A broadly tunable perovskite for efficient planar heterojunction solar cells," *Energy & Environmental Science*, vol. 7, no. 3, pp. 982-988, 2014.

[40] M. Tabassum, Q. Zia, J. Li, M. T. Khawar, S. Aslam, and L. Su, "$FAPbBr_3$ perovskite nanocrystals embedded in poly(l–lactic acid) nanofibrous membranes for enhanced air and water stability," *Membranes (Basel)*, vol. 13, no. 3, 2023.

[41] Z. Zhou, S. Pang, F. Ji, B. Zhang, and G. Cui, "The fabrication of formamidinium lead iodide perovskite thin films via organic cation exchange," *Chemical Communications*, vol. 52, no. 19, pp. 3828-3831, 2016.

[42] K. Hills-Kimball, Y. Nagaoka, C. Cao, E. Chaykovsky, and O. Chen, "Synthesis of formamidinium lead halide perovskite nanocrystals through solid-liquid-solid cation exchange," *Journal of Materials Chemistry C. Materials*, vol. 5, no. 23, pp. 5680-5684, 2017.

[43] W. Wang, Y. Wu, D. Wang, and T. Zhang, "Effective control of the growth and photoluminescence properties of $CsPbBr_3$/Cs_4PbBr_6 nanocomposites by solvent engineering," *ACS Omega*, vol. 4, no. 22, pp. 19641-19646, 2019.

[44] Y. L. Tong, Y. W. Zhang, K. Ma, R. Cheng, F. Wang, and S. Chen, "One-step synthesis of FA-directing $FAPbBr_3$ perovskite nanocrystals toward high-performance display," *ACS Applied Materials & Interfaces*, vol. 10, no. 37, pp. 31603-31609, 2018.

[45] S. Zhang, and C. Wang, "Precise analysis of nanoparticle size distribution in TEM image," *Methods and Protocols*, vol. 6, no. 4, p. 63, 2023.

[46] Y. Zu, J. Xi, L. Li, J. Dai, S. Wang, F. Yun, B. Jiao, H. Dong, X. Hou, and Z. Wu, "High-brightness and color-tunable $FAPbBr_3$ perovskite nanocrystals 2.0 enable ultrapure green luminescence for achieving recommendation 2020 displays," *ACS Applied Materials & Interfaces*, vol. 12, no. 2, pp. 2835-2841, 2020